Journal of Neuroscience Methods 139 (2004) 99–109

JOURNAL OF NEUROSCIENCE METHODS

www.elsevier.com/locate/jneumeth

A laser micromachined probe for recording multiple field potentials in the thalamus

You-Yin Chen [a], Te-Son Kuo [a,b], Fu-Shan Jaw [b,*]

[a] *Institute of Electrical Engineering, National Taiwan University, No. 1, Sect. 4, Roosevelt Road, Taipei 106, Taiwan ROC*
[b] *Institute of Biomedical Engineering, College of Medicine, National Taiwan University, No. 1, Sect. 1, Jen-Ai Road, Taipei 100, Taiwan ROC*

Received 18 February 2004; received in revised form 14 April 2004; accepted 19 April 2004

Abstract

Multichannel recording provides integral information about electrical brain activities at one instant in time. In this study, multielectrode probes were fabricated to record the thalamic field potentials (FPs) responding to the electrical stimulation of nerve at the rat tail. At first, the number of sweeps used to form the evoked FP average and the spatial sampling density were determined by using cross-correlation functions, which were then statistically analyzed. The difference was significant at $P < 0.05$, if the number of sweeps for averaging was more than 50 and the spatial interval between two consecutive recording sites was less than 50 μm in the anteroposterior, mediolateral and ventrodorsal directions. The responsive area was distributed vertically in the thalamus (ventral posterior lateral (VPL) nucleus); therefore, the recording sites were arranged in one linear array. Sixteen recording sites, which were 50 μm apart from each other, were distributed in the ventrodorsal direction. A 16-channel silicon probe was fabricated by using a standard photolithography process and laser micromachining techniques. The probe provides capabilities to record multiple thalamic evoked FPs and multiunit activities simultaneously.

Keywords: Field potential; Thalamus; Cross-correlation; Multielectrode probe; Laser micromachining

1. Introduction

The brain includes billions of intricately connected neurons, and the central nervous system must be able to process complex sensory information simultaneously when stimuli are present (Schouenborg et al., 1986). The thalamus operates as a relay station to transfer sensory information from the periphery to the related region of cerebral cortex to make into even higher level of perception (Jones, 1985; Kandel et al., 1991). Sensory information generated by integrating electronic potentials, with countless temporal and spatial variations, is simultaneously collected through the volume conductor of several neural activities (Plonsey and Barr, 2000). For this, multielectrode recordings (Buzsáki et al., 1989; Starr et al., 1973; Sugihara et al., 1995) have been used to observe the activities of groups of neurons and provide information about the distribution and functions of areas responding to particular stimulation such as pain (Chudler and Dong, 1983), touch (Di and Barth, 1991), and sound (Barth et al., 1993).

Multichannel electrodes include those developed to record from peripheral nerve tissues (Akin et al., 1994; Bradley et al., 1997; Edell, 1986; Mannard et al., 1974; Mensinger et al., 2000), from cultured nerve tissues (Jimbo and Robinson, 2000; Maher et al., 1999; Pine, 1980) and from central nervous tissues in vivo (BeMent et al., 1986; Hetke et al., 1994; Wise and Angell, 1975; Wise et al., 1970). Because various neural tissues are specially oriented and distinct in their anatomic location, these multichannel electrodes are specially designed to meet the spatial requirements to cover the responsive area in the brain. Therefore, the first consideration in fabricating multichannel electrodes is the spatial arrangement of the recording sites, which is determined by the anatomic structure of the neural tissues to be recorded. In previous work, the depth of the thalamic ventral posterior lateral (VPL) nucleus, the area responding to stimulation of the rat tail, was found to be distributed vertically and 5–6 mm from the surface of the cerebral cortex (Chen, 1998; Emmers, 1988). In layered structures like the cerebral cortex or thalamus, multichannel electrodes

* Corresponding author. Tel.: +886-2-2312-3456x1453; fax: +886-2-2394-0049.
E-mail address: irradiance@so-net.net.tw (F.-S. Jaw).

0165-0270/$ – see front matter © 2004 Elsevier B.V. All rights reserved.
doi:10.1016/j.jneumeth.2004.04.022

placed perpendicular to the layers at different depths will allow recording sites to be matched to the geometry of the neural circuit more accurately. These can be used to for stereotaxic analysis or for current source density (CSD) analysis.

Spatial resolution is an important aspect for designing multielectrode probes. If the interval between recording sites is too wide, the tiny responsive area may be missed, resulting in distorted or unreliable information (Roberts and Scher, 1982; Taccardi et al., 1994). If the interval is too narrow, more recording sites are required to cover the entire responsive area. Although additional details of the distribution of neural signals can be obtained, more data are required and signal processing is complicated. Also, more sophisticated fabrication of multichannel electrodes is needed because of the high-integral-density layout. Therefore, objective guidelines for the spatial interval between recording sites are needed for fabricating multielectrode probes. In this study, the cross-correlation function was used to determine an optimal interval between recording sites (Amzica and Steriade, 2000; Contreras et al., 1997; Destexhe et al., 1999; Steriade et al., 1996a, 1996b). If two recording sites are placed some distance apart on a nerve fiber, the cross-correlation function calculated for the two signals recorded from these electrodes will typically show peaks for both positive and negative lags. The fact that the function is sensitive to the direction of lag is important in the context of neural signal analysis (Challis and Kitney, 1990).

Signal averaging is commonly applied to increase the signal-to-noise ratio (SNR) of evoked field potentials (FPs) (Rompelman and Ros, 1986). For a reasonable number of sweeps in the average, the average evoked potential (AEP) is a more accurate reflection of the true evoked potential (Turetsky et al., 1988). Therefore, we can measure the reliability of the AEP by computing the cross-correlation between two AEPs with the same sweeps (Mocks et al., 1984; Turetsky et al., 1988). In the current research, the cross-correlation function is used to estimate the minimum number of sweeps needed to average FPs; such correlations are considered statistically significant at a confidence level of 95%.

Among the micromachined silicon probes provided by the University of Michigan, NIH NCRR Center for Neural Communication Technology (CNCT), type *5mm50* possesses the longest shaft with a length of 5 mm, which is unfortunately unable to reach most of the thalamus. Therefore, we applied micromachining technology to fabricate a probe suitable for mapping the evoked thalamic potential contour. The following factors were considered: (1) the shape of the electrode, which depends on the recording site (i.e. anatomic arrangement of neurons to be recorded); (2) the recording range; (3) the recording interval (i.e. distance between electrodes); and (4) the electrode material. The main task was to set the spatial interval between each pair of recording sites and to determine the number of sites needed to cover the entire responsive area.

2. Materials and methods

2.1. Animal preparation

The study was approved by the Committee of Animal Experimentation at the National Taiwan University. Twenty-five adult male Wistar rats weighing 350–450 g (Animal Center of the National Taiwan University Hospital) were anesthetized with ketamine (50 mg/kg i.p.). The trachea, femoral artery and vein were cannulated to maintain anesthesia with the continuous delivery of low-dose ketamine (15 mg/mL, 1 mL/h i.v.) through an infusion pump. The rectal temperature of rats was maintained at 38 °C during the surgical procedure with the use of a heat blanket and a homeothermic blanket control unit (Model 734, Harvard Apparatus Inc., USA). The animals were placed on a stereotaxic apparatus (Model 900, David Kopf, USA) to enable microscopic dissection. The exposed brain was covered with warm liquid paraffin (34 °C) in oil pools formed by the cut skin. The rats were maintained under physiologic conditions (mean blood pressure >90 mmHg, end tidal CO_2 concentration of 3–4.5%).

2.2. Stimuli and recording

A microelectrode was mounted on a tri-axis manipulator (Model 1460, David Kopf) with 10-μm resolution along each axis, positioned over the exposed brain, and inserted into the responsive area (thalamic VPL nucleus). Stainless steel needles were inserted into the left side of the tail between the S_2 and S_3 segments, and a pulse of 5–10 V with a 100 μs duration was delivered at 1 Hz (Digitimer DS2 and Axon isolator 11; Digitimer Ltd, UK). An audio monitor (AM8, Grass Instruments, USA) and an oscilloscope (TDS 420A, Tetronix, USA) were used to locate the thalamic area responding to electrical stimulation. Thalamic FPs were recorded, amplified with a gain of 2500, filtered through a pass-band from 0.01 to 300 Hz (five-pole Butterworth filter), simultaneously, and digitized at 3000 Hz by using a 12-bit analog-to-digital (AD) conversion card (PCI-MIO-16E-4, National Instruments, USA) sequentially. The 16 signals were multiplexed at the channel switching rate of 500 kHz. Multiunit activities (MUAs) also were recorded, amplified with a gain of 5000, filtered (three-pole Bessel filter) through a pass-band from 100 to 5000 Hz, and digitally sampled at 50 000 Hz by using an AD converter card (PCI-MIO-16E-4, National Instruments). Data were analyzed offline by using MATLAB (MATLAB R12, Mathworks Inc., USA) to evaluate the evoked responses induced by electrical stimuli.

2.3. Determination of the neural recording criteria

Two important recording parameters were determined before the multielectrode probe was fabricated. The first was the number of sweeps (*N*) evoked FPs per site; we could increase the SNR by averaging successive FPs evoked with

the electrical stimuli. The second was the spatial interval (D) between two adjacent recording sites. Parameters were identified on the basis of the cross-correlation function, which shows more sensitivity to differences in the pattern and time lags than the amplitude of the signals. The values of cross-correlation functions were expressed as the mean ± S.D. Student's paired t-test was used to evaluate differences in correlation. A value of $P < 0.05$ was considered to indicate a statistically significant difference.

Ten male Wistar rats were used to determine N and D in the electrophysiologic experiment as described in Sections 2.1 and 2.2. Evoked FPs were recorded with glass micropipettes filled with 3 M NaCl solution (3–5 MΩ), and the recordings were amplified and digitized for storage and analysis. To determine a reasonable number of sweeps (N), a total of $2N$ repetitions of electrical stimulations were applied to the rat tail with a frequency of 1 Hz. The data were digitized at a fixed rate (a time interval of 1/3000th of a second). A total of M data points (in this study, $M = 512$) were recorded for each sweep. The data corresponding to the first N sweeps were denoted as follows: $X_n[t_m]$, where $n = 1 - N$ and $m = 1 - M$. These were the reference data. The data corresponding to the remaining N sweeps were denoted as follows: $Y_n[t_m]$. Then, the cross-correlation (ρ) associated with the number of sweeps N was calculated as shown (Challis and Kitney, 1990)

$$\bar{X}_{t_m} = \frac{1}{N}\sum_{n=1}^{N} X_n[t_m], \qquad \bar{Y}_{t_m} = \frac{1}{N}\sum_{n=1}^{N} Y_n[t_m],$$

$$\bar{X} = \frac{1}{M}\sum_{m=1}^{M} \bar{X}_{t_m}, \qquad \bar{Y} = \frac{1}{M}\sum_{m=1}^{M} \bar{Y}_{t_m},$$

$$\rho = \frac{(1/(N-1))\sum_{m=1}^{M}(\bar{X}_{t_m} - \bar{X})(\bar{Y}_{t_m} - \bar{Y})}{\sqrt{(1/(N-1))\sum_{m=1}^{M}(\bar{X}_{t_m} - \bar{X})^2 (1/(N-1))\sum_{m=1}^{M}(\bar{Y}_{t_m} - \bar{Y})^2}}$$

where $X_n[t_m]$ and $Y_n[t_m]$ are evoked FPs at time t_m and sweep n. $\bar{X}_{t_m}$, $\bar{Y}_{t_m}$, $\bar{X}$, and $\bar{Y}$ are the means of $X_n[t_m]$, $Y_n[t_m]$, $\bar{X}_{t_m}$, and $\bar{Y}_{t_m}$, respectively.

Fig. 1A presents three pairs of evoked responses with different averaging numbers. The fastest component responding to the electrical stimulation of the rat tail was observed at around 22 ms. The resulting waveforms indicated that more sweeps averaged over the evoked FPs corresponded to a higher ρ. Consistent with statistical convention, 50 sweeps was determined for the average FP at each recording site with a mean correlation coefficient of 0.98 ± 0.01 ($n = 10$; $P < 0.05$) (Fig. 1B).

Time relations between two adjacent sites were revealed by the cross-correlation function, which provides information about the degree of resemblance and phase sign as well as the time-lags separating two evoked FPs. Therefore, parameters $X_n[t_m]$ and $Y_n[t_m]$ in the equations just described

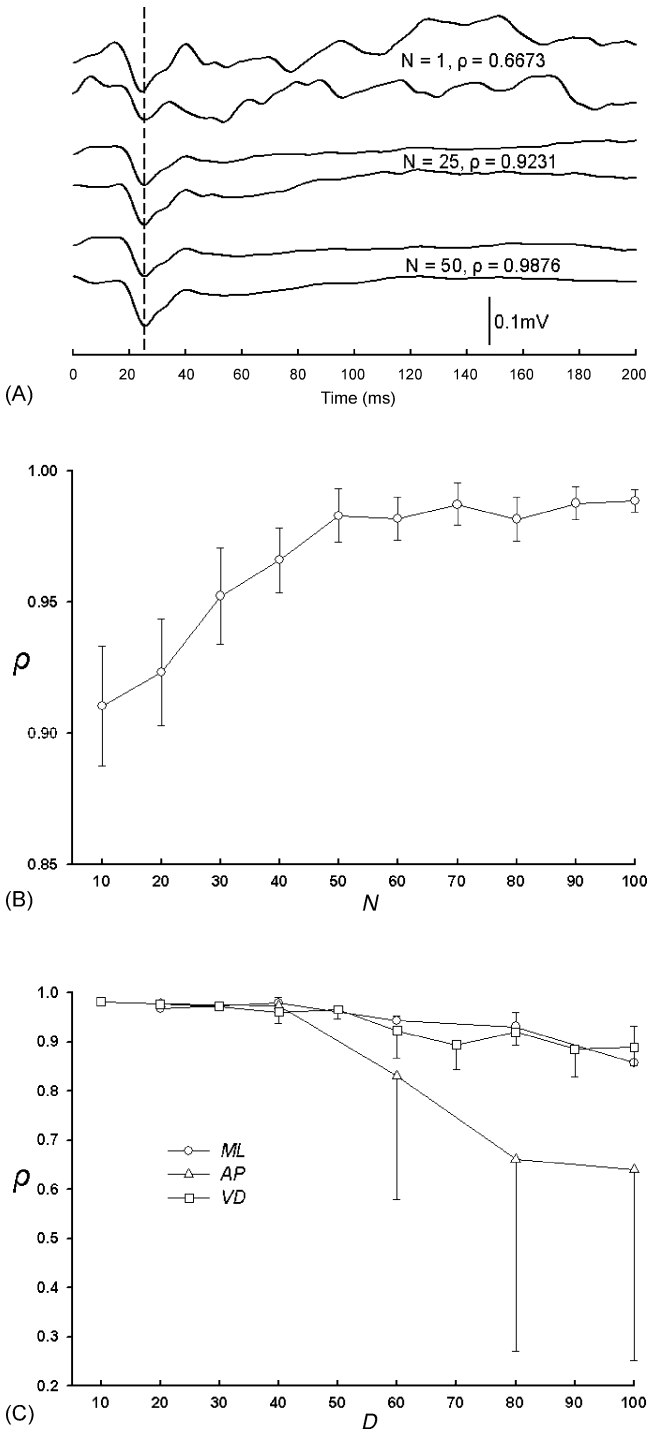

Fig. 1. Effects of number averaging of evoked FPs and the interelectrode distance between two consecutive recording sites on ρ. (A) Plot shows the averaged evoked FPs after different numbers of averages. The upper two waveforms show typical FPs with a single sweep ($n = 1$). Variation (background noise) among FPs is relatively large compared with that of the lower waveforms, which used more trials to average signals. The fastest component was observed at around 22 ms (dashed line). (B) Plot shows the relationship between mean correlation coefficient ρ and the number of sweeps for averaging evoked FPs. (C) Effects of interelectrode distances on mean correlation coefficient ρ along each axis: ML, AP, and VD.

represented the measured data corresponding to two adjacent recording sites. The number of sweeps (N) was set to 50. Spatial interval of sampling was verified in the mediolateral (ML), anteroposterior (AP), and ventrodorsal (VD) directions (Paxinos and Watson, 1986). The mean correlation coefficients were 0.98 ± 0.01 ($n = 10$; $P < 0.001$) at 60 μm, 0.96 ± 0.04 ($n = 10$; $P < 0.05$) at 50 μm, and 0.97 ± 0.01 ($n = 10$; $P < 0.001$) at 50 μm for the ML, AP, and VD directions, respectively (Fig. 1C).

2.4. Estimations of SNR

The AEP still includes some spontaneous activity "noise", which has no time-locked relationship to the stimulus, though noise is diminished by averaging evoked potentials to enhance the SNR. Therefore, if $X_n[t_m]$ is the evoked FP described in Section 2.3, unbiased estimates of noise power (σ_N^2), signal power (σ_S^2), and SNR can be calculated as follows (Mocks et al., 1984; Turetsky et al., 1988):

$$\bar{X}_{t_m} = \frac{1}{N}\sum_{n=1}^{N} X_n[t_m],$$

$$\sigma_N^2 = \frac{1}{M(N-1)}\sum_{n=1}^{N}\left(\sum_{m=1}^{M}(X_n[t_m] - \bar{X}_{t_m})^2\right),$$

$$\sigma_S^2 = \frac{1}{M}\sum_{m=1}^{M}\bar{X}_{t_m}^2 - \frac{1}{N}\sigma_N^2,$$

$$\mathrm{SNR} = \frac{\sigma_S^2}{\sigma_N^2}$$

where σ_N^2 is the power of background activities and measurement error, and σ_S^2 is the power of the true signal of the AEPs.

2.5. Fabricating the multielectrode probe

The main design elements of the probe were as follows (Fig. 2A): (a) fine, needle-like shafts were designed to penetrate the neural tissue with the least damage. (b) For acute implantation, platinum conductors (15 μm × 15 μm per site) were placed over the outermost section of the shafts to serve as microelectrode contacts to detect the neural signals. The optimal interval between adjacent recording sites was set to 50 μm that appeared to provide adequate spatial interval of sampling in the thalamic VPL. (c) Contact pads for external electrical interconnection used wire bonding via a PC board. AutoCAD (AutoCAD 2002, Autodesk Inc., USA) was used to layout more than 30 multielectrode probe patterns onto the masks (Fig. 2B). Table 1 lists the probe specifications.

The multielectrode probes were fabricated on a silicon substrate (4 in., 100 oriented, P type) by using three

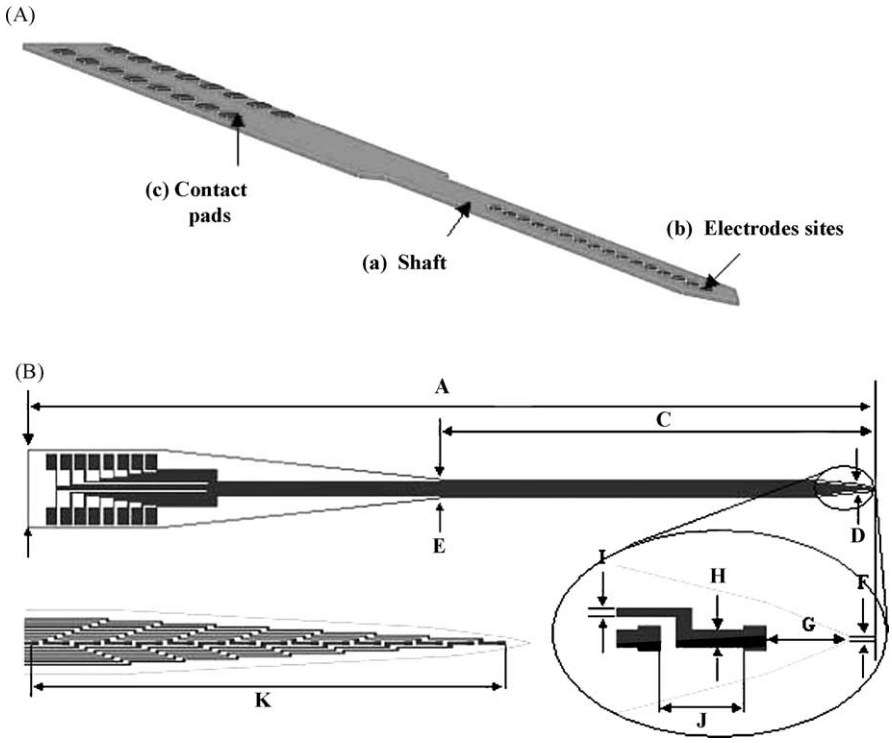

Fig. 2. (A) Schematic view of the multielectrode probe structure (not to scale). (B) AutoCAD layout shows that the probe has integrated connector pads, a long shaft and recording sites. The tip of the probe was designed with a 30° taper angle.

Table 1
Specifications of the multielectrode probe

Dimension	Value
Number of sites	16
Site area (μm^2)	225
Probe length (A) (mm)	11.85
Probe width (B) (mm)	1
Shaft length (C) (mm)	6
Shaft width (D, E) (μm)	40 220
Tip width (F) (μm)	3
Distance (G) (μm)	50
Wire width (H) (μm)	10
Wire width (I) (μm)	5
Electrode distance (J) (μm)	50
Recording length (K) (μm)	974

Note: The letters in parentheses correspond to the letters shown in Fig. 2B.

photomasks. The probe fabrication process proceeded in five phases (Fig. 3). The first mask generated the shape of the probe, including its length and the angle of its tip. The second formed the patterns of the recording sites, contact pads, and interconnect traces. The third determined the patterns of the recording sites and the contact pads. Two layers (1500 Å silicon nitride at 800 °C and 5000 Å polysilicon at 620 °C) were initially deposited onto the wafer by using a low-pressure, chemical-vapor deposition (LPCVD) reactor (SRC, NCTU, Taiwan; Fig. 3A). $POCl_3$ doping was performed by using an oxidation and diffusion furnace (No. 55667, LINDBERG, USA) with annealing (4 h) to reduce the resistance of the polysilicon. Sheet resistance, as assessed by using four-point probe measuring system (RT-7, Napson, Japan), was as low as 10–11 Ω/■.

When the photoresistor (FH-6400, FUJIFILM Arch, Japan) was spun on the wafer, the second mask was aligned and exposed. The polysilicon reactive ion etching (poly-RIE) system (RIE-10N, SAMCO, Japan) was used to etch the 5000 Å of polysilicon to create the structural elements, recording sites, interconnect traces, and contact pads (Fig. 3B). Silicon nitride (3000 Å) was deposited as a protective layer by using a plasma-enhanced chemical vapor deposition (PECVD) system (BR-2000LL, NARC, Taiwan). Another photoresistor (FH-6400L, FUJIFILM Arch) was spun on the wafer, and the third mask was aligned and exposed. Windows (3000 Å) were opened to the polysilicon layer by using dielectric RIE (RIE200L, SAMCO) to form the recording sites and contact pads (Fig. 3C). A photoresistor (AZ-P6112, Clariant, Japan) was spun on the wafer, and the third mask was aligned and exposed again. Titanium/platinum (2000 Å/2000 Å) metallization layers were evaporated with the dual E-Gun evaporation system (EBX-10C, ULVAC, Japan). Then, the lift-off process was applied to determine the recording sites and contact pads (Fig. 3D). The 6-μm-thick photoresistor (AZ-P6420, Clariant, Japan) was spun on the wafer, and the first mask was aligned and exposed to outline the appropriate shape. Etching was performed to a depth of 10 μm by using a dielectric RIE (RIE200L, SAMCO) (Fig. 3E).

The last stage of the fabrication is to shape the multielectrode probe into a long with a thin shaft and needle-like tip. Laser machining technology can be used conveniently to cut through the materials and thus generate slots of various shapes, including rectangular, round, hexagonal, and other shapes.

A YAG laser (SC150, Trend Laser Tech, Taiwan) was used to shape the shaft. The laser system generated low power (65 W) with a 1.064-μm wavelength to ablate the probes from the wafer. With a focusing length of 60 mm, the spot of the laser beam had a diameter of 75 μm (rms), yielding a high power density, a narrow line and a high micro-marking capacity for ablating the probes from the edges cut by the laser. A gas jet exerts a mechanical force that ejects the melt from the cut zone, which it cools by forced convection, to remove the melt caused by laser cutting. Inefficient removal of the molten layer can degrade the cut surface (Chen et al., 2000).

After the probes were ablated from the wafer, they were mounted on PC boards with Au wire bonding (No. 242627B, West Bond, USA). The probe base and wire bonds were smeared with waterproofing glue (Hot Melt 3748V0, 3M, USA).

3. Results

3.1. Number of evoked FPs to be averaged and spatial interval

The cross-correlation function was used to determine the number of sweeps in averaging FPs. The value of ρ increased rapidly with N, when N was less than 50; ρ exhibited no significant improvement when N exceeded 50 (Fig. 1B). To achieve reliable evoked FP waveforms, the minimum number of sweeps N_{min} was set to be 50, which resulted in a mean correlation coefficient of 0.98 ± 0.01 ($n = 10$; $P < 0.05$).

The correlation function was also used to determine the sampling distance D. Fig. 1C shows that the mean correlation coefficient diminished with increasing interelectrode spacing, especially in the AP direction. The mean correlation coefficient was of 0.96 ± 0.04 ($n = 10$; $P < 0.05$) when sampling distance in the AP direction was 50 μm. However, the mean of ρ was decreased to a value of 0.64 ± 0.39 ($n = 10$; $P > 0.05$) when D was 100 μm. The rapid decrease in ρ along the AP axis might have been due to its coincidence with the pathway of the medial lemniscus. Hence, a small displacement in this direction might have caused a large variation in the evoked FPs recorded. The maximum spatial interval D_{max} along each axis was set to 50 μm to prevent spatial aliasing errors.

3.2. Electrical characteristics of the laboratory-designed probe

Fig. 4A and B displays micrographs of the first prototype of the laboratory-designed probe. Fig. 4A shows melt

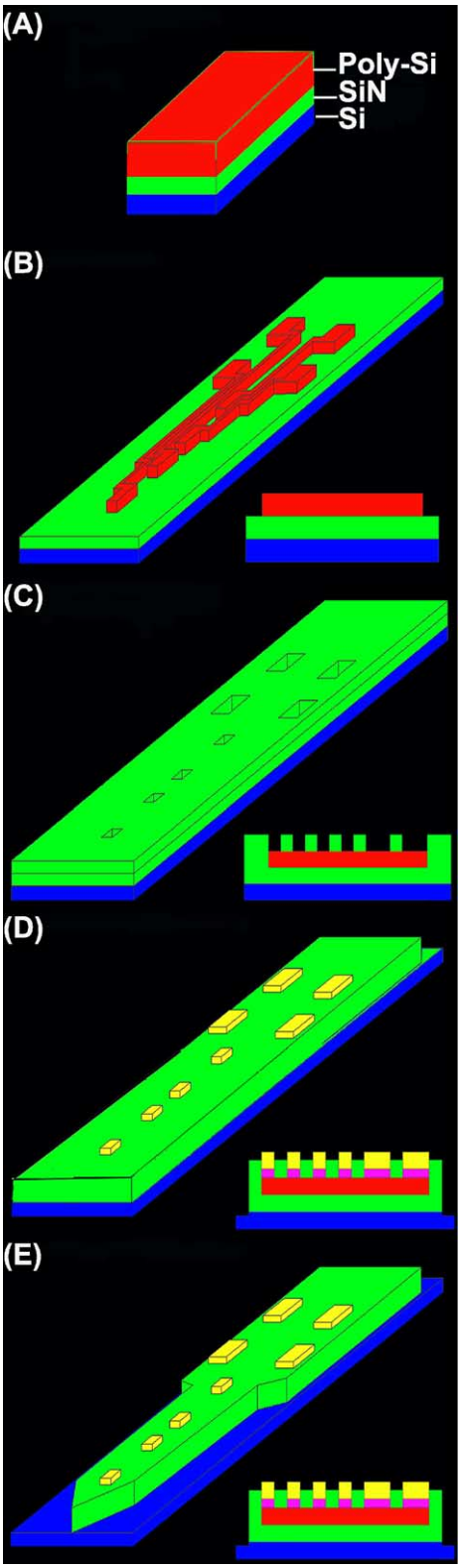

Fig. 3. Diagram illustrates fabrication of the multielectrode probe (not to scale). (A) Deposition of two layers: Si_3N_4, and polysilicon. (B) RIE-etching of the polysilicon layer. (C) Nitride deposition and RIE etching to form the electrode and pad holes. (D) Metallization (platinum/titanium) deposition and lift off. (E) Shape of the probe is etched by using RIE.

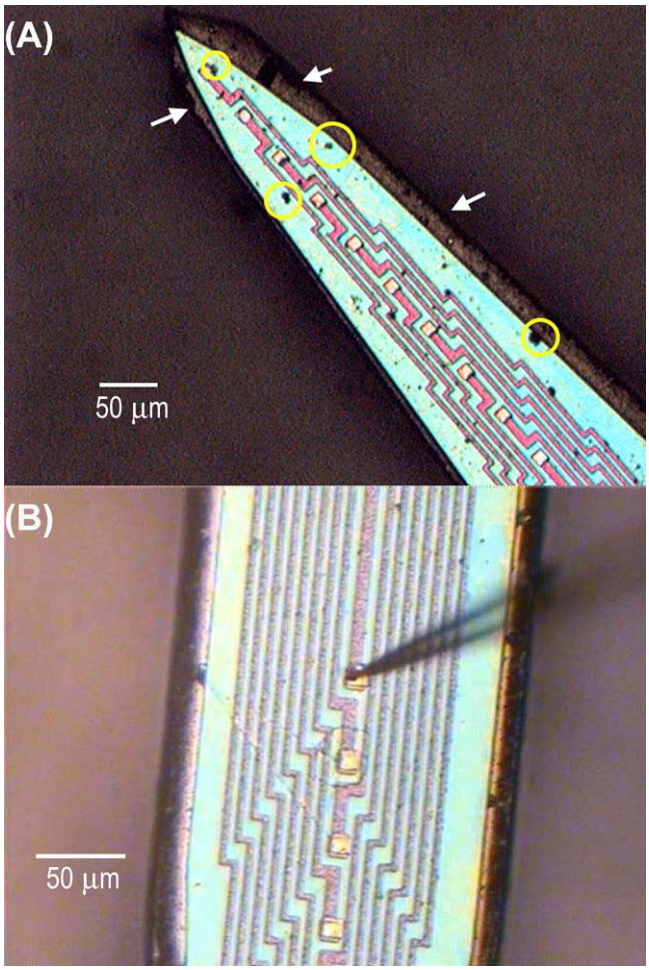

Fig. 4. Detailed view of the multielectrode probe. (A) The pitch of the recording sites is 50 μm. The surface of the recording sites is evaporated with platinum (silver squares), and the interconnect traces are structured with polysilicon (pink lines). The melt articles are marked with yellow circles. The residual space, which consisted of oxide and melt, are located around the edge of the probe after laser cutting (arrows). (B) The melt particles are removed by using SPM, and one microprobe was touched the recording site to measure the resistance between the recording electrode and the contact pad.

deposited around the shaft. This oxide was formed by the interaction of the laser and the silicon nitride at high temperature on the surface of the probe during cutting. Because melt particles on the surface could have compromised signal recording, they were wiped off by wet cleaning (SPM, H_2SO_4/H_2O_2, 80 °C) after the probe were ablated from the wafer (Fig. 4B).

Bench-top measuring setups were used to confirm the electrical functionality of the laboratory-designed probe. A dc probe station (BD-8, Everybing, Taiwan) was used to measure the resistance of the 16 groups of recording electrode-contact pads. Test results indicated the resistance of each group is $27.93 \pm 0.42\,k\Omega$ ($n = 16$). Impedance spectroscopy (LCR821, Instek, Taiwan) was also used to examine the probes which were placed in physiologic saline solution (0.9% NaCl) at room temperature in vitro. The

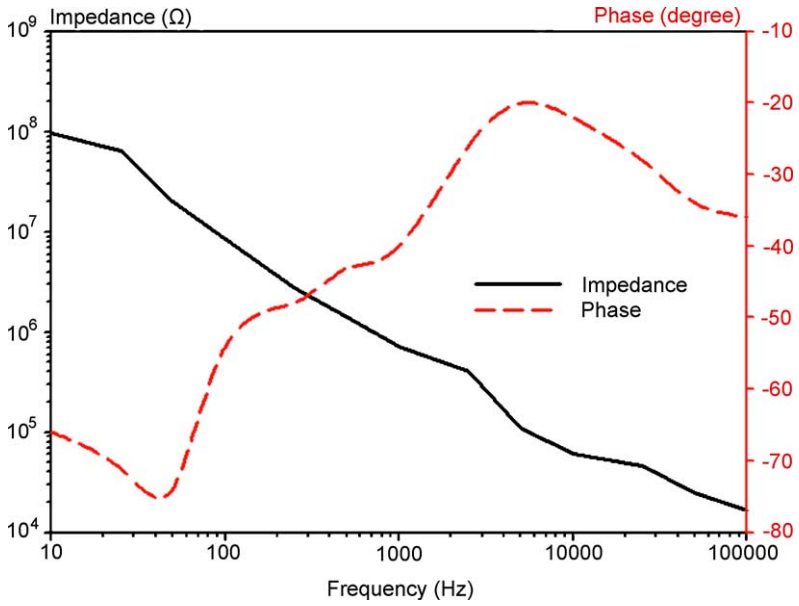

Fig. 5. Impedance spectroscopy of the multielectrode probe shows the impedance spectrum (black line) and the phase spectrum (red line).

impedance of shafts with 16 electrodes was measured with a sinusoidal voltage source (100 mV, 50 nA, and 10–10^5 Hz) with respect to a large reference electrode (silver wire). Fig. 5 shows typical impedance spectrographs. The magnitude of impedance decreased as the frequency of the ac signal increased. The impedance was approximately 100 MΩ with phase −66° when the frequency was 10 Hz, whereas the impedance decreased to 0.72 MΩ with phase −40° when frequency was increased to 1000 Hz.

3.3. Comparison with the performance of various electrodes in vitro and in vivo testing

We also measured the impedance of a CNCT probe (type *5mm50*, 177 μm^2 per electrode), a quartz-platinum/tungsten microelectrode (outer shaft diameter of 100 μm; Thomas Recordings, Germany), and a glass micropipette (tip diameter 15 μm, AM System, USA) in vitro at the test signal frequency of 1000 Hz (sine wave). Impedance spectroscopy was performed as before. Impedances of the CNCT probe, quartz-platinum/tungsten microelectrode and glass micropipette were 1.82 MΩ (phase, −82°), 0.25 MΩ (phase, −15°), and 2.1 MΩ (phase, −54°), respectively.

To estimate SNRs of thalamic FPs recorded by using a CNCT probe, a laboratory-designed probe, a platinum/tungsten microelectrode, and a glass micropipette was used to evaluate the changes in the SNRs of AEPs with respect to various number of sweeps (a novel method described in Section 2.4). The duration of evoked FPs recorded by the four types of electrodes was about 150 ms. Fig. 6 shows the SNRs, which are represented by $10\log(\sigma_S^2/\sigma_N^2)$, were plotted against the number of sweeps. SNR increased when the number of sweeps in averaging increased. The value of the SNR increases slowly when the number of sweeps is more than 60. A larger recording site generally yields a higher SNR.

Comparisons of the impedance (from in vitro testing) and SNRs (from in vivo testing) associated with different electrodes indicted that the laboratory-designed probe performed better than the CNCT probe and the glass micropipette and only slightly worse than the platinum/tungsten microelectrode.

3.4. Neural recording

The laboratory-designed probe was used to record thalamic evoked responses. Ten male rats underwent the electrophysiologic procedures, as described before. A probe assembly was mounted on the manipulator, positioned over the exposed brain and inserted into the area of the thalamus that responds to electrical stimulation of the S_2–S_3 segments of the rat tail. The signal at the deepest electrode on the shaft that was monitored during insertion by using the oscilloscope and audio system.

The neural recording demonstrated that the laboratory-designed probe could record evoked responses in the thalamic VPL nucleus. Fig. 7 shows MUAs and evoked FPs (average of 50 sweeps) in rat 3. MUAs and evoked FPs were closely related, with units discharging with high preference during FP negativity.

By using the laboratory-designed probe to record evoked FPs in response to stimuli, the locations of the neural generators could be identified precisely with CSDs calculated with the Poisson equation (Mitzdorf, 1985; Nicholson and Freeman, 1975; Townsend et al., 2002). Fig. 8A shows that the recording sites in relation to the different thalamic layers were identified in the coronal section (100 μm thick, Nissl substance) stained with cresyl violet. Fig. 8B shows

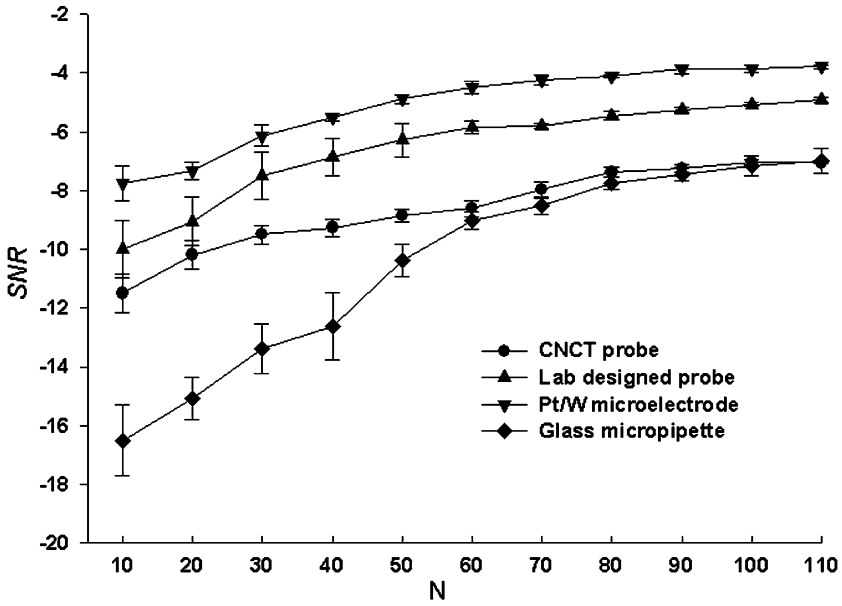

Fig. 6. SNR of evoked FPs recorded from four types of electrodes plotted against various sweeps to average evoked FPs ($n = 5$). As the number of sweeps increases, the SNR corresponding to different electrodes also increases. The SNR curve approaches the plateau when the number of sweep is more than 60 and the level of SNR plateaus is higher by the increase of the electrode surface.

the evoked FPs recorded simultaneously from 16 electrodes distributed with a 50 μm pitch. The earliest components of average evoked FPs arrived at 25 ms after stimulation, and the maximum negative FPs were in the thalamic VPL, which was at a depth of 5950–6000 μm from the cortical surface. Fig. 8C shows the one-dimensional CSDs, which yielded spatial profiles of extracellular current sinks and sources along the axis of the electrode array. The recording area was small; therefore, tissue conductivity was assumed to be homogeneous across various depths (Ahrens and Freeman, 2001; Townsend et al., 2002), especially in the VPL nucleus (Chen, 1998; Emmers, 1988). CSD analysis revealed that the earliest sinks in VPL, sinks 2 and 4, were at depths of 5750 and 6000 μm from the cortical surface, respectively; these arrived at 25 ms after stimulation. Shortly after 15 ms, sink 3 shifted toward the upper layer of the VPL at 5950 μm from the cortical surface. One later sink in the posterior thalamus, sink 1, was 5600 μm from the cortical surface and arrived 40 ms after stimulation.

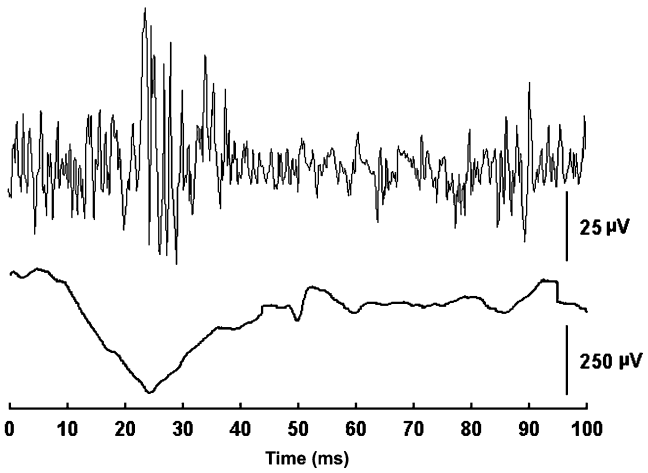

Fig. 7. Representative examples show that MUAs (upper waveform) and evoked FPs (lower waveform) were recorded from the laboratory-designed probe. Evoked FPs and MUAs were highly correlated.

4. Discussion

4.1. Probe specification based on optimal criteria of recording thalamic evoked FPs

Previous reports of probe fabrication (Kewley et al., 1997; Najafi et al., 1985; Norlin et al., 2002) discussed only differences in techniques and did not mention how to set the suitable probe specifications for microfabrication. In this study, the probe was fabricated on the basis of a reasonable specification to ensure reliable recording of neural activities. The specification included the length of the shaft of the probe and the interval between two adjacent recording sites. However, the latter, which is used to determined the density of spatial sampling, is more important. In previous studies, a frequency-domain method was used to estimate the maximum interelectrode spacing (Freeman and Nicholson, 1975). In this study, a time-domain method (the cross-correlation function) was applied to determine the optimal spatial interval of sampling. Our results suggest that the spatial interval along the *x*, *y*, and *z* directions should be 50–60 μm, which is not far from that decided by Freeman and Nicholson (1975). In addition, other groups have also applied the concept of the correlation function to address

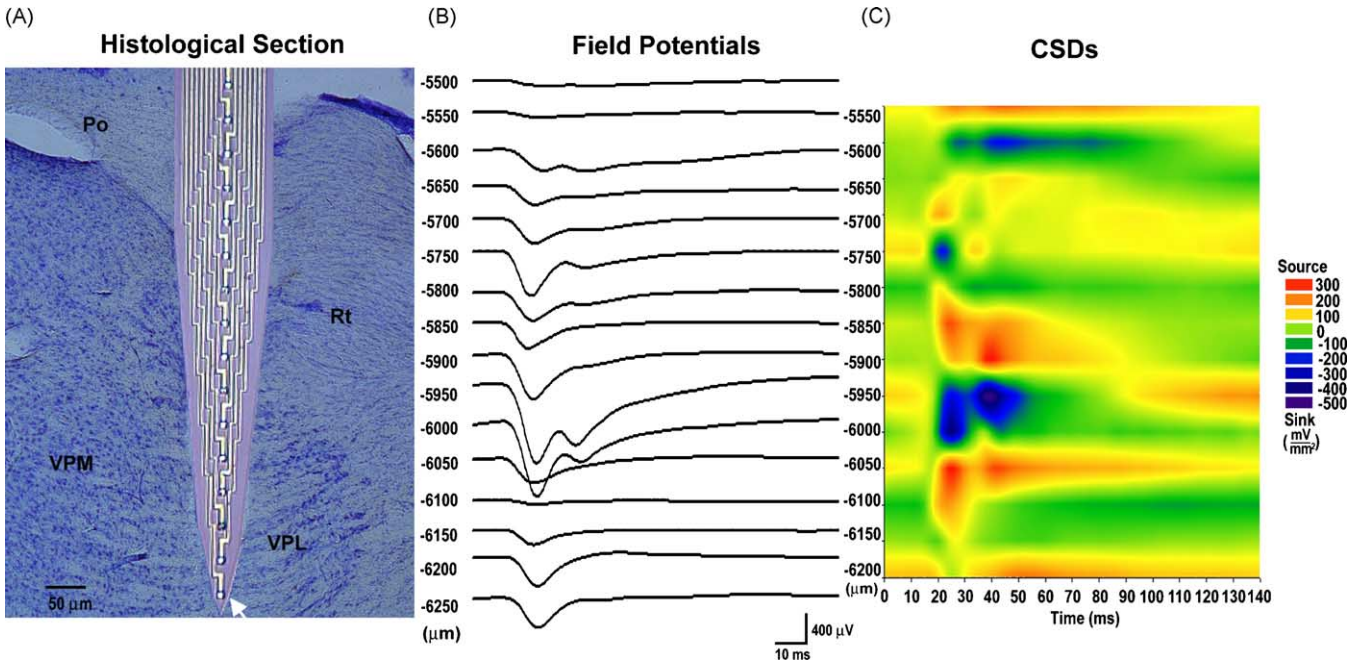

Fig. 8. (A) Coronal section at AP level −3.5 mm shows the in situ location of the probe and recording sites. Po indicates the posterior thalamus nuclear group; Rt, reticular thalamus nucleus and VPM, ventral posteromedial thalamus nucleus. (B and C) The deepest electrode (arrow) was 6250 μm from the brain surface. The recording range of the 16 electrodes covered 750 μm vertically. Laminar profiles of average evoked FPs (B) and CSDs (C) were acquired in the VPL nucleus. (B) Average evoked-FP (50-sweep) profile at 50-μm intervals shows that components of the evoked FPs had different negative amplitude-vs.-depth profiles, suggesting their generation by different synapses and in different layers. (C) One-dimensional CSD map derived from thalamic evoked FPs in (B) and provided precise locations of sinks (numbered 1–4) with respect to anatomic layers shown in (A).

the spatial interval of sampling ECG signals (Botteron and Smith, 1996; Kadish et al., 1999).

4.2. Techniques for shaping probe

For fabricating a multielectrode probe with a long, thin shaft and a sharp, needle-like tip, the pivotal step is defining its shape. Deep boron diffusion (approximately 15 μm) has to define the overall shape (Najafi et al., 1985). Deep reactive ion etching (DRIE) has also been applied to shape the probes on the front side of a wafer (Kewley et al., 1997). The probes were released from the wafer by using ethylene diamine pyrochatechol (EDP) etching (Najafi et al., 1985) or an RIE etchant in conjunction with backside-wet etching

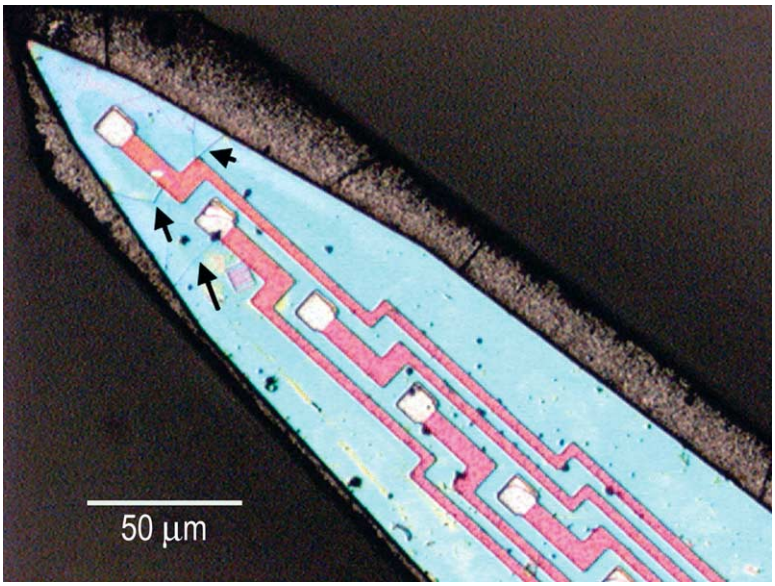

Fig. 9. Microcracks distributed on the outermost aspect of the shaft (arrows).

techniques (Kewley et al., 1997; Norlin et al., 2002). Another approach uses (1 1 0)-oriented wafers and anisotropic wet etching, which stops on the (1 1 1) planes, to define the sidewalls of the shaft (Clark, 1990). Although the use of chemical wet etching to shape the probe has several advantages (e.g. low cost, high reliability, high productivity, excellent etching selection ratio), it also has following shortcomings: (1) It requires deionized water and a reaction solution, which adds cost. (2) The chemicals (e.g. potentially explosive waste gas) create a safety issue. (3) The attachment of photoresistance is another issue. (4) Etching may be incomplete or uneven if the solution does not contact completely with the surface of the chip.

The key feature in our fabrication process was the application of laser micromachining for defining the shape. This approach yielded sharp tips without additional steps and could generate various shapes (e.g. rectangles, circles, hexagons). Compared with traditional chemical etching, laser cutting is easier and less time-consuming. It also eliminates the need to control production conditions, and increases yield rate (>85%). Once the patterns and parameters are programmed into the computer, the wafer is positioned, and automatic cutting begins. The process can be fully computerized and automated, and the manufacturing time is shortened. Other advantages include no mask needed, no contamination, and having an ability of multidirectional cutting with a micron-grade accuracy. It is believed that this is the first time the laser-cutting technique has been applied in this field.

However, an engineering challenge remains. Microcracks may develop during unstable cutting or cutting under improper conditions. Occasionally, these cracks cut off the interconnect traces as indicated by the arrows in Fig. 9. Therefore, processing parameters, such as the distribution and intensities of the power, cutting speed, and shape of the beam, must be prudently selected.

4.3. Capability of the laboratory-designed probe

The laboratory-designed probe stably recorded FPs and MUAs and reached the responsive area in the thalamus (VPL nucleus). Furthermore, the distance between recording sites can be determined more accurately and used in CSD analysis or stereotaxic analysis of a highly structured area of the brain, such as layers of the cortex and thalamus.

4.4. Future work

The laboratory-designed probe displaced more neural volume and caused more neural damage during penetration of the cerebral cortex to reach the thalamus, which is located in a deep part of the brain. Compared with the CNCT probe, which caused damage of a <50-μm track (Townsend et al., 2002), our probe produced more substantial damage (>200-μm track) and dimpling (Kewley et al., 1997). As a result, we did not use backside wet-etching to diminish the thickness of the laboratory-designed probe (200 μm). Therefore, a new fabrication process with backside wet-etching is being developed to reduce the thickness to achieve a truly thin-film probe.

The three-dimensional distribution was such that a single-shaft neural probe could not cover its entirety. Future designs will include multiple parallel shafts (Kewley et al., 1997; Rousche and Normann, 1992) with fixed intervals referring to the ML or AP recording intervals. A forked shape will also be incorporated to record spatial and temporal neural activity in the responsive area of the brain.

Acknowledgements

The authors thank Dr. Nan-Nong Huang for the helpful review of the manuscript; Mr. Pai-Feng Yang for helping with the histological procedures; and the University of Michigan CNCT (http://www.engin.umich.edu/facility/cnct/) sponsored by NIH/NCRR grant P41-RR09754 for providing silicon probes. This work was financially supported by the National Science Council of the Republic of China, Taiwan, contract NSC-91-2213-E-002-119.

References

Ahrens KF, Freeman WJ. Response dynamics of entorhinal cortex in awake, anesthetized, and bulbotomized rats. Brain Res 2001;911:193–202.

Akin T, Najafi K, Smoke RH, Bradley RM. A micromachined silicon sieve electrode for nerve regeneration applications. IEEE Trans Biomed Eng 1994;41:305–13.

Amzica F, Steriade M. Neuronal and glial membrane potentials during sleep and paroxysmal oscillations in the neocortex. J Neurosci 2000;20:6648–65.

Barth DS, Kithas J, Di S. Anatomic organization of evoked potentials in rat parietotemporal cortex: somatosensory and auditory responses. J Neurophysiol 1993;69:1837–49.

BeMent SL, Wise KD, Anderson DJ, Najafi K, Drake KL. Solid-state electrodes for multichannel multiplexed intracortical neuronal recording. IEEE Trans Biomed Eng 1986;33:230–41.

Botteron GW, Smith JM. Quantitative assessment of the spatial organization of atrial fibrillation in the intact human heart. Circulation 1996;93:513–8.

Bradley RM, Cao X, Akin T, Najafi K. Long term chronic recordings from peripheral sensory fibers using a sieve electrode array. J Neurosci Methods 1997;73:177–86.

Buzsáki G, Bickford RG, Ryan LJ, Young S, Prohaska O, Mandel RJ, et al. Multisite recording of brain field potentials and unit activity in freely moving rats. J Neurosci Methods 1989;28:209–17.

Challis RE, Kitney RI. Biomedical signal processing (in four parts). Part 1. Time-domain methods. Med Biol Eng Comput 1990;28:509–24.

Chen K, Lawrence YY, Modi V. Gas jet–workpiece interactions in laser machining. J Manuf Sci Eng 2000;122:429–38.

Chen YY. MS thesis. Current source density of field potentials in the brain. Taipei, Taiwan: National Taiwan University; 1998.

Chudler EH, Dong WK. The assessment of pain by cerebral evoked potentials. Pain 1983;16:221–44.

Clark LD. Ph.D. dissertation. System for chronic neural signal transduction processing and control. Boston: Massachusetts Institute of Technology; 1990.

Contreras D, Destexhe A, Steriade M. Spindle oscillations during cortical spreading depression in naturally sleeping cats. Neuroscience 1997;77:933–6.

Destexhe A, Contreras D, Steriade M. Spatiotemporal analysis of local field potentials and unit discharges in cat cerebral cortex during natural wake and sleep states. J Neurosci 1999;19:4595–608.

Di S, Barth DS. Topographic analysis of field potentials in rat vibrissa/barrel cortex. Brain Res 1991;546:106–12.

Edell DJ. A peripheral nerve information transducer for amputees: long-term multichannel recordings from rabbit peripheral nerves. IEEE Trans Biomed Eng 1986;33:203–14.

Emmers R. Somesthetic system of the rat. New York: Raven Press; 1988. p. 9–39.

Freeman JA, Nicholson C. Experimental optimization of current source–density technique for anuran cerebellum. J Neurophysiol 1975;38:369–82.

Hetke JF, Lund JL, Najafi K, Wise KD, Anderson DJ. Silicon ribbon cables for chronically implantable microelectrode arrays. IEEE Trans Biomed Eng 1994;41:314–21.

Jimbo Y, Robinson HP. Propagation of spontaneous synchronized activity in cortical slice cultures recorded by planar electrode arrays. Bioelectrochemistry 2000;51:107–15.

Jones EG. The thalamus. New York: Plenum Press; 1985.

Kadish A, Hauck J, Pederson B, Beatty G, Gornick C. Mapping of atrial activation with a noncontact, multielectrode catheter in dogs. Circulation 1999;99:1906–13.

Kandel ER, Schwartz JH, Jessell TM. Principles of neural science, third ed. New York: Elsevier Science; 1991.

Kewley DT, Hill MD, Borkholder DA, Opris IE, Manluf NI, Storment CW, et al. Plasma-etched neural probe. Sens Actuators A Phys 1997;58:27–35.

Maher MP, Pine J, Wright J, Tai YC. The neurochip: a new multielectrode device for stimulating and recording from cultured neurons. J Neurosci Methods 1999;87:45–56.

Mannard A, Stein RB, Charles D. Regeneration electrode units: implants for recording from single peripheral nerve fibers in freely moving animals. Science 1974;183:547–9.

Mensinger AF, Anderson DJ, Buchko CJ, Johnson MA, Martin DC, Tresco PA, et al. Chronic recording of regenerating VIIIth nerve axons with a sieve electrode. J Neurophysiol 2000;83:611–5.

Mitzdorf U. Current source–density method and application in cat cerebral cortex: investigation of evoked potentials and EEG phenomena. Physiol Rev 1985;65:37–100.

Mocks J, Gasser T, Pham DT. Variability of single visual evoked potentials evaluated by two new statistical tests. Electroencephalogr Clin Neurophysiol 1984;57:571–80.

Najafi K, Wise KD, Mochizuki T. A high-yield IC-compatible multichannel recording array. IEEE Trans Electron Devices 1985;32:1206–11.

Nicholson C, Freeman JA. Theory of current source–density analysis and determination of conductivity tensor for anuran cerebellum. J Neurophysiol 1975;38:356–68.

Norlin P, Kindlundh M, Mourouxl A, Yoshida K, Hofman UG. A 32-site neural recording probe fabricated by DRIE of SOI substrates. J Micromech Microeng 2002;12:414–9.

Paxinos G, Watson C. The rat brain in stereotaxic coordinates, second ed. New York: Academic Press; 1986.

Pine J. Recording action potentials from cultured neurons with extracellular microcircuit electrodes. J Neurosci Methods 1980;2:19–31.

Plonsey R, Barr RC. Bioelectricity: a quantitative approach, second ed. New York: Kluwer Academic/Plenum Publishers; 2000. p. 266–71.

Roberts DE, Scher AM. Effect of tissue anisotropy on extracellular potential fields in canine myocardium in situ. Circ Res 1982;50:342–51.

Rompelman O, Ros HH. Coherent averaging technique: a tutorial review. Part 1: Noise reduction and the equivalent filter. J Biomed Eng 1986;8:24–9.

Rousche PJ, Normann RA. A method for pneumatically inserting an array of penetrating electrodes into cortical tissue. Ann Biomed Eng 1992;20:413–22.

Schouenborg J, Kalliomaki J, Gustavsson P, Rosen I. Field potentials evoked in rat primary somatosensory cortex (SI) by impulses in cutaneous A beta- and C-fibres. Brain Res 1986;397:86–92.

Starr A, Wise KD, Csongradi J. An evaluation of photoengraved microelectrodes for extracellular single-unit recording. IEEE Trans Biomed Eng 1973;20:291–3.

Steriade M, Amzica F, Contreras D. Synchronization of fast (30–40 Hz) spontaneous cortical rhythms during brain activation. J Neurosci 1996a;6:392–417.

Steriade M, Contreras D, Amzica F, Timofeev I. Synchronization of fast (30–40 Hz) spontaneous oscillations in intrathalamic and thalamocortical networks. J Neurosci 1996b;16:2788–808.

Sugihara I, Lang EJ, Llinas R. Serotonin modulation of inferior olivary oscillations and synchronicity: a multiple-electrode study in the rat cerebellum. Eur J Neurosci 1995;7:521–34.

Taccardi B, Macchi E, Lux RL, Ershler PR, Spaggiari S, Baruffi S, et al. Effect of myocardial fiber direction on epicardial potentials. Circulation 1994;90:3076–90.

Townsend G, Peloquin P, Kloosterman F, Hetke JF, Leung LS. Recording and marking with silicon multichannel electrodes. Brain Res Protoc 2002;9:122–9.

Turetsky BI, Raz J, Fein G. Noise and signal power and their effects on evoked potential estimation. Electroencephalogr Clin Neurophysiol 1988;71:310–8.

Wise KD, Angell JB. A low-capacitance multielectrode probe for use in extracellular neurophysiology. IEEE Trans Biomed Eng 1975;22:212–9.

Wise KD, Angell JB, Starr A. An integrated-circuit approach to extracellular microelectrodes. IEEE Trans Biomed Eng 1970;17:238–47.